

The role of hydrous phases in the formation of trench parallel anisotropy: Evidence from Rayleigh waves in Cascadia

Lara S. Wagner,¹ Matthew J. Fouch,² David E. James,² and Maureen D. Long³

Received 18 March 2013; revised 26 April 2013; accepted 29 April 2013.

[1] The cause of seismic anisotropy exhibiting trench parallel fast directions in subduction systems has been the subject of significant recent research. We provide new constraints on the contributions of hydrous phases to seismic anisotropy from an unusually well-localized region of trench parallel fast directions in Rayleigh wave phase velocities near the Cascade arc at 45 to 66 s periods. We constrain the location of the anisotropic material to within or directly above the oceanic plate, using the depth sensitivity of Rayleigh waves as a function of frequency and the accurate slab imaging available for Cascadia from scattered wave studies. We infer that the likely source of trench-parallel anisotropy is either a thin layer of sheared hydrous material directly above the slab or hydrated outer rise faults in the upper part of the subducting plate. Similar contributions to trench parallel anisotropy from hydrous phases are likely stronger in other subduction zones.

Citation: Wagner, L. S., M. J. Fouch, D. E. James, and M. D. Long (2013), The role of hydrous phases in the formation of trench parallel anisotropy: Evidence from Rayleigh waves in Cascadia, *Geophys. Res. Lett.*, 40, doi:10.1002/grl.50525.

1. Introduction

[2] Seismic anisotropy is often used to constrain upper mantle flow patterns, following the assumption that the observed anisotropy is due to the preferred alignment of olivine fast axes in the direction of shearing within the shear plane [e.g., *Karato et al.*, 2008]. In the simplest model, subduction zone flow patterns are controlled by the coupling of the downgoing plate to the overriding asthenospheric mantle, which would produce dominantly trench normal corner flow in the mantle wedge. This scenario provides a ready explanation for the typical observations of trench normal SKS fast splitting directions in subduction zone back arcs [*Long and Silver*, 2008] if we assume the presence of A-, C-, or E-type olivine fabric, for which the fast splitting direction tends to align in the direction of horizontal mantle

flow [*Karato et al.*, 2008] via crystallographic preferred orientation (CPO).

[3] One intriguing wrinkle to this simple model has been the observation of trench parallel fast directions in subduction zone fore arcs [*Long and Silver*, 2008], primarily from SKS shear wave splitting studies. Several possible explanations exist for these widespread (but not universal) observations, each of which places the anisotropic material at a different range of upper mantle depths [e.g., *Jung and Karato*, 2001; *Faccenda et al.*, 2008; *Long and Silver*, 2008; *Healy et al.*, 2009; *Katayama et al.*, 2009; *Nikulin et al.*, 2009; *Jung*, 2011]. These explanations can roughly be divided into two categories. The models in the first category invoke some form of CPO in asthenospheric olivine. For example, the formation of olivine B-type fabric in the shallow mantle wedge, which predicts fast directions orthogonal to the direction of mantle flow [*Jung and Karato*, 2001], could produce trench parallel anisotropy in subduction zone fore arcs [*Kneller et al.*, 2005; *Kneller et al.*, 2008]. Similarly, a pressure-induced transition to B-type olivine fabric, proposed by *Jung et al.* [2009], would predict dominantly trench parallel fast directions beneath the slab for the case of 2-D entrained subsurface flow. Other explanations have invoked the more prevalent A-type (or similar) fabrics along with generally trench parallel mantle flow patterns, either above or below the subducting plate [e.g., *Long and Silver*, 2008]. Anisotropy may also be present in lithospheric mantle of the slab itself as a result of fossil spreading normal to the ridge [e.g., *Song and Kim*, 2012; *Audet*, 2013], although for many regions (including Cascadia), this geometry is unlikely to produce a trench parallel fast direction.

[4] Models in the second category attribute some or all of trench parallel anisotropy to the presence of mantle hydrous phases (e.g., antigorite, chlorite, talc) [e.g., *Reynard*, 2012]. While the elastic properties of these phases have been less thoroughly studied than those of olivine, existing research suggests they are generally highly anisotropic [e.g., *Mainprice and Ildefonse*, 2009]. The CPO of phyllosilicates likely results in the preferential orientation of seismically slow *c* axes normal to the planes of foliation [*Katayama et al.*, 2009; *Jung*, 2011; *Mainprice and Ildefonse*, 2009; *Bezacier et al.*, 2010]. Models within this category differ from each other primarily in the distribution of the relevant hydrous phases within the subduction system. Proposed anisotropic hydrated regions within subduction zones include a layer along the interface between the overriding continental crust and the subducting oceanic crust [*Park et al.*, 2004; *Nikulin et al.*, 2009], a layer located directly above the subducting oceanic crust farther down dip beneath the mantle nose or wedge [*Katayama et al.*, 2009; *Jung*, 2011; *Kneller et al.*, 2005], and along deep outer rise fault planes in the slab that trend parallel to the trench. In the case of hydrated outer

Additional supporting information may be found in the online version of this article.

¹Department of Geological Sciences, University of North Carolina, Chapel Hill, North Carolina, USA.

²Department of Terrestrial Magnetism, Carnegie Institution of Washington, Washington, District of Columbia, USA.

³Department of Geology and Geophysics, Yale University, New Haven, Connecticut, USA.

Corresponding author: L. S. Wagner, Department of Geological Sciences, University of North Carolina at Chapel Hill CB# 3315 Chapel Hill, NC 27599, USA (wagner@unc.edu)

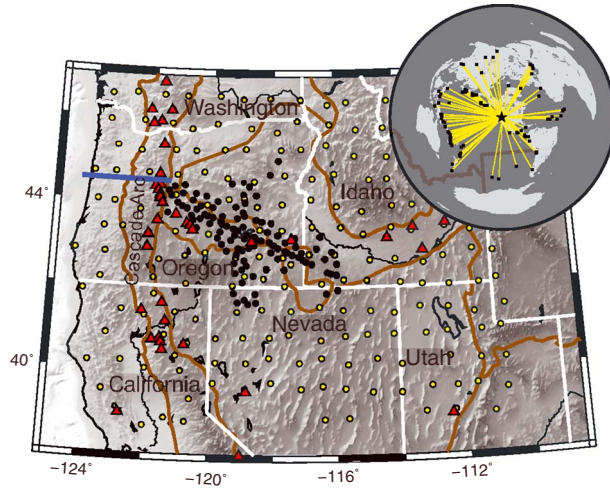


Figure 1. Map of study area. The gray background shows topography and white lines indicate state boundaries. Brown lines indicate boundaries between geologic provinces. Yellow circles indicate station locations from the Transportable Array used in this study. Black circles show the stations used from the High Lava Plains deployment. Red triangles show Holocene volcanoes. The blue line indicates the approximate location of the cross section in Figure 3. The inset map shows the (black squares) locations of earthquakes used in this study and the (yellow lines) great circle paths to the study area.

rise faults, anisotropy can be due to either the combined crystallographic and shape-preferred orientation (SPO) of multiple hydrated fault surfaces [Faccenda *et al.*, 2008] and/or to the ongoing dehydration of hydrous phases in these fault zones and associated increased pore pressure and crack damage [Healy *et al.*, 2009].

[5] Previous studies of SKS splitting in Cascadia have found evidence for dominantly plate motion parallel fast splitting directions [Currie *et al.*, 2004], and thus Cascadia has been considered one of only a few exceptions to the rule of dominantly trench parallel SKS splitting in subduction zone fore arcs worldwide [Long and Silver, 2008]. A possible explanation for the lack of trench parallel fast directions in Cascadia invokes the unusually high temperatures that result from the subduction of a very young slab [Peacock *et al.*, 2002], which would inhibit the formation of B-type olivine fabric and limit the presence of stable hydrous phases at depth.

[6] Here we present evidence for a localized region of trench parallel anisotropy in the Cascadia subduction zone (Figure 1) from inversions of Rayleigh wave phase velocities. Unlike SKS splitting measurements, which are sensitive to an integrated view of anisotropy from the core-mantle boundary to the surface, Rayleigh waves are sensitive to a limited range of depths in the upper mantle that vary according to frequency [Saito, 1988] (Figure 2). This feature allows us to identify regions of trench-parallel anisotropy whose SKS splitting signal might be overprinted by stronger trench normal anisotropy at other depths and to place constraints on which processes are more or less likely to have a significant effect on the formation of trench parallel anisotropy in Cascadia.

2. Methods

[7] The data and methodology for this study build on earlier phase velocity inversions [Wagner *et al.*, 2010] that use the

finite frequency two-plane wave tomography methodology [Forsyth and Li, 2005; Yang and Forsyth, 2006]. Seismic stations used are from the EarthScope Transportable Array (rows E–Q, columns 1–17) and from 116 stations of the High Lava Plains deployment (Figure 1). We analyzed all events with a magnitude greater than 6.3 between 22° and 130° epicentral distance from the center of the study area (Figure 1, inset). Each event was analyzed at 12 different periods ranging from 33 to 143 s. New to this study is the ability to determine the spatial variability of anisotropy directions and magnitudes instead of solving for a single pair of best fit anisotropy terms at each period, as shown in Wagner *et al.* [2010]. Grid node locations are determined by establishing a pole of rotation due north of, and 90° away from, the center of the array. Grid nodes are then placed at evenly spaced increments of azimuth and great circle distance from the poles [Forsyth and Li, 2005]. We use a grid node spacing of 0.66° for anisotropy parameters, which corresponds to an average intermodal distance of approximately 75 km. Phase velocities at any location are approximated by

$$C(\omega, \theta) = B_0(\omega) + B_1(\omega)\cos(2\theta) + B_2(\omega)\sin(2\theta)$$

[8] omitting the higher-order 4θ terms which have been shown to have little effect for Rayleigh waves [Smith and Dahlen, 1973; Weeraratne *et al.*, 2007]. At each anisotropy grid node, we solve for B_1 and B_2 . Starting anisotropy values are set to zero unless otherwise noted. The fast direction of propagation is defined as $0.5 \times \arctan(B_2/B_1)$, and the peak-to-peak degree of anisotropy is given by $2 \times (B_1^2 + B_2^2)^{1/2}$.

3. Results

[9] Our primary observations are shown in Figure 2 and Supplementary Figure 1. At 33 s, anisotropic fast directions vary smoothly across the arc, trending E-W to NE-SW from southern to northern Oregon. Between 45 and 66 s, we observe generally E-W (trench normal) fast directions across central and eastern Oregon, while just east of the arc, the magnitude of the observed anisotropy is strongly reduced. Just west of the arc, in contrast, we observe a striking pattern of N-S trending (trench parallel) fast directions with relatively large amplitudes (2%–3%). This trench parallel anisotropy is again reduced to negligible levels slightly farther west toward the trench. This pattern of abrupt rotation from trench normal to trench parallel fast directions is no longer visible at periods of 77 s and longer and is replaced by a pattern of relatively smoothly varying NE-SW trending fast directions in the fore arc into E-W in the back arc.

[10] Our results at periods between 45 and 66 s are different from the SKS splitting results of Currie *et al.* [2004], who find roughly trench normal trending fast directions at stations DBO (in southwestern Oregon) and PIN (just east of the arc in central Oregon). Currie *et al.* [2001] find evidence from local shear wave splitting for trench parallel fast directions in the crust (where we have little sensitivity), though most of their measurements are north of our study area. Park *et al.* [2004] analyze anisotropy at station COR (Figure 1, along our blue line, near longitude -123° W), using receiver functions and finding a dipping layer with a slow axis oriented approximately trench parallel at a depth of ~ 40 km. This is consistent with our observed E-W oriented fast directions at 33 s.

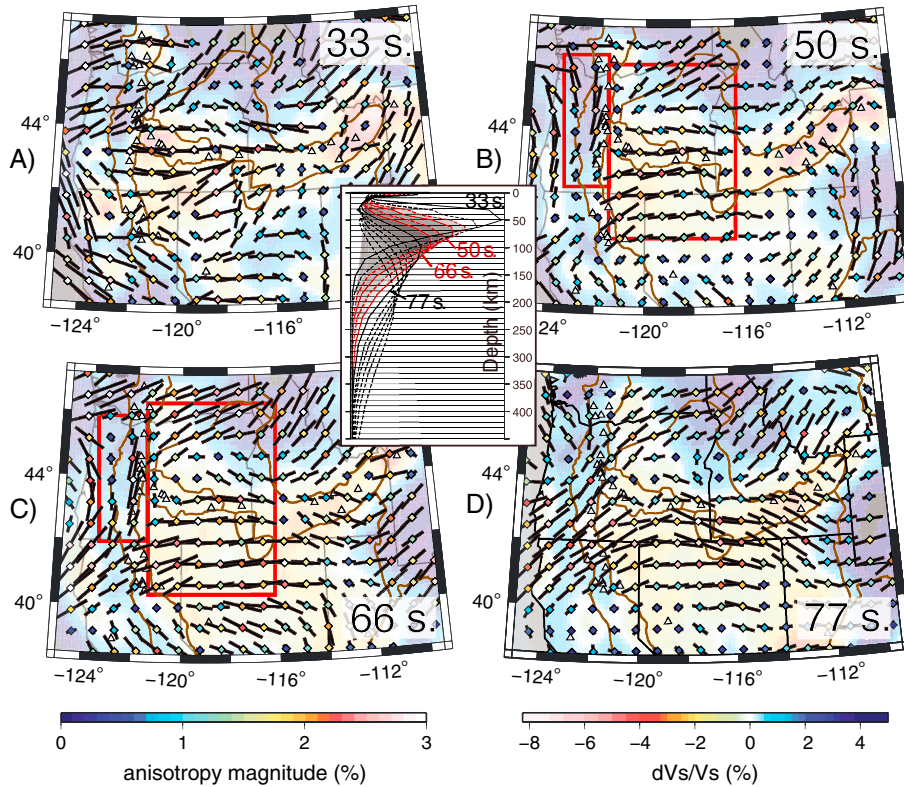


Figure 2. Results of inversions for anisotropic Rayleigh wave phase velocities. Results are shown at four different periods: 33, 50, 66, and 77 s. The faint background colors indicate isotropic phase velocity deviations. Fast directions are indicated by the direction of the black lines. Magnitude of anisotropy is shown both by the length of the line and by the color of the diamond. The boxes indicate areas of trench parallel or trench normal fast directions. The central inset shows the relative sensitivity of each period to shear wave velocities at depth. (a–d) Periods shown have solid lines; other periods are dashed. Those periods with trench parallel fast directions are plotted in red, and the area under their curves are colored with transparent black shading. All other periods are plotted with black lines, and the areas under their curves are colored with transparent white shading above the transparent black shading mentioned above.

[11] In order to test our ability to constrain such an abrupt change in anisotropic magnitude and azimuth, we repeated our inversions with different starting models for anisotropy. In one inversion, we introduced a strong (5%) N-S trending anisotropy into the starting model and in another inversion a strong (5%) E-W trending anisotropy. The anisotropy results for these inversions are shown in Supplementary Figure 2. While the outermost edges of our study area show a strong dependence on starting model, the spatial pattern of trench parallel, null, and trench normal fast directions beneath the Cascade arc are remarkably consistent for different starting models, demonstrating that our data can indeed resolve this feature.

4. Discussion

[12] Determining the cause of our trench parallel observations requires constraints on both depth and the location of the anisotropic material relative to local subduction zone geometry. To this end, we compare results from scattered wavefield imaging [Rondenay *et al.*, 2001; Bostock *et al.*, 2002] across the Cascades at 44.5°N to our results at anisotropy grid nodes that lie directly along this transect (Figures 1 and 3). The central grid node exhibits trench parallel anisotropy at 45–66 s periods, but other periods at this grid node, and all other periods at the other grid nodes, show either trench normal anisotropy or little to no azimuthal anisotropy at all.

[13] We now consider what periods and grid nodes we would expect to exhibit trench parallel anisotropy given the most common explanations for this phenomenon. B-type fabric generated within the mantle wedge should produce trench parallel anisotropy in both of the two easternmost grid nodes that sample the wedge. For the central node, the periods which most strongly sample the mantle wedge are 33 and 40 s. One possible explanation is that the trench parallel signal at these periods is overridden by a strong trench normal component in the lower crust to which they are sensitive but longer periods are not. However, studies of crustal anisotropy in Cascadia indicate weak trench parallel anisotropy in the crust [Currie *et al.*, 2001], which would add to the observed trench parallel anisotropy, not reduce it. Anisotropy generated either within or beneath the hydrated wedge “nose,” and anisotropy associated with hydration along the interplate boundary, would be expected to produce trench parallel anisotropy only in the westernmost grid node. Anisotropy caused by a pressure-induced B-type fabric transition at a depth of ~90 km [Jung *et al.*, 2009] would be observed at all grid nodes at equal periods, and anisotropy caused by slab flow should be observed at periods over 45 s in the westernmost grid node and at periods over 77 s in the central grid node. We do not observe trench parallel anisotropy at any of these periods/grid nodes.

[14] The dashed green box in Figure 3 is drawn to identify the region that is not excluded by the considerations

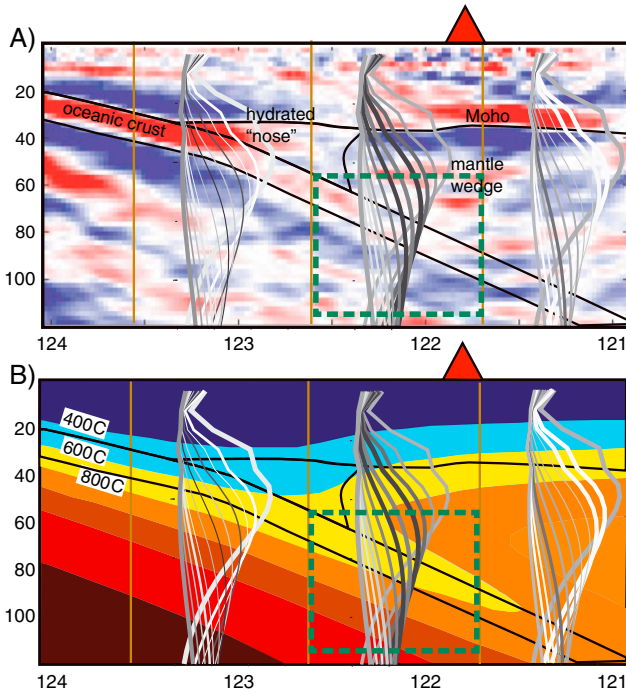


Figure 3. Possible causes of trench parallel anisotropy. In each plot, we show the sensitivity kernels at each period for which we inverted at the three grid nodes that overlap with the scattered wave image [Rondenay *et al.*, 2001] whose (a) location is indicated in Figure 1 by the blue line. The line weight of the sensitivity curves is scaled by the magnitude of the anisotropy at that period at that grid node (heavier lines indicate higher magnitudes). The color of the lines indicates azimuth, with black indicating N-S trending anisotropy and white indicating E-W trending anisotropy. (Figure 3a and 3b) Vertical brown lines show halfway points between the grid node locations. (Figure 3a and 3b) Thin black lines are interpretations of structures along the scattered wave profile [Bostock *et al.*, 2002]. (Figure 3b) The colors show temperature contours along this same profile [Bostock *et al.*, 2002]. The large red triangles show the approximate location of the Cascade arc. The green box indicates the most likely source region for the observed trench parallel anisotropy (see text for details).

discussed above as the principal source of the observed trench parallel anisotropy. The most notable feature that we see within the green box is the 800°C isotherm surrounding the relatively cold descending oceanic crust and thin layer of adjacent asthenospheric mantle (Figure 3b). In this region, between 600°C and 800°C, hydrous phases in the oceanic crust, such as glaucophane and lawsonite, are no longer stable [Hacker, 2008], and the most stable remaining mantle hydrous phase is chlorite [van Keken *et al.*, 2011; Wada *et al.*, 2012]. At these pressures, the highest temperature at which chlorite would be stable is ~800°C [van Keken *et al.*, 2011; Wada *et al.*, 2012]. This suggests two possible sources for the observed trench parallel anisotropy: (1) a thin layer of chlorite above the subducting Juan de Fuca slab at 60–90 km depth and/or (2) the dehydration of chlorite in outer rise faults below the oceanic crust.

[15] Previous studies have suggested trench parallel fast SKS splitting observations with delay times over 1 s could be caused at least in large part by the formation of a layer

of antigorite above the subducting plate [e.g., Katayama *et al.*, 2009]. While the CPO of chlorite has not yet been studied, both chlorite and antigorite have similar single crystal anisotropies and are both hydrous sheet silicates [Mainprice and Ildefonse, 2009]. Studies indicate simple shear deformation of antigorite results in the slow c axis oriented perpendicular to the plane of foliation (the shear plane) [e.g., Katayama *et al.*, 2009]. If we assume that chlorite and antigorite have similar CPOs and assume that the plane of foliation is (nearly) isotropic [Bezacier *et al.*, 2010], then the magnitude of the predicted azimuthal anisotropy induced by chlorite CPO would be strongly controlled by the dip angle of the slab. If the foliation plane is not isotropic and aligns either a axis or b axis with a trench-normal lineation direction [Katayama *et al.*, 2009; Jung, 2011], then the influence of slab dip would be decreased or increased, respectively. Assuming that chlorite behaves similarly to antigorite, our trench parallel observations could be explained by a thin layer of this hydrous phase sheared along the top of the subducted plate. However, this anisotropy signal would be localized and could easily be overprinted by a strong trench normal anisotropic signal elsewhere (e.g., below the slab) for SKS phases, resulting in the observed trench normal SKS fast splitting directions in Cascadia.

[16] The second possible contributing factor is the presence of hydrous phases in aligned outer rise faults in the subducted plate. Nedimovic *et al.* [2009] find evidence for hydrated faults extending into the mantle lithosphere within the Juan de Fuca plate in proximity of the trench. Faccenda *et al.* [2008] propose that a combination of CPO and shape-preferred orientation (SPO) caused by hydrous minerals in subducted outer rise faults could be the main source of trench parallel SKS splitting in most subduction zones. They argue that the absence of trench parallel SKS in Cascadia is due to the high temperatures that would cause dehydration within outer rise faults at shallower depths. However, chlorite is likely stable over some depth range in our area of interest within the slab, and though the CPO of chlorite is not known, it is known to have far lower shear wave velocities than dry peridotite [Mainprice and Ildefonse, 2009]. This implies that at a minimum, the SPO suggested by Faccenda *et al.* [2008] would be expected to generate a (possibly weak) trench parallel signal. Additionally, crack damage due to increased pore pressure from progressive dehydration reactions can also contribute to trench parallel anisotropy [Faccenda *et al.*, 2008; Healy *et al.*, 2009]. This effect is expected to exist only within those portions of the slab undergoing dehydration reactions, so areas farther downdip would not be expected to exhibit similar trench parallel anisotropy, consistent with our results.

[17] Finally, we note that our ability to image this trench parallel anisotropy in Cascadia is due to our ability to isolate a relatively small depth range as the likely source. This is in part due to the depth dependence of Rayleigh wave sensitivity, but it is also in part due to the absence of other significant potential sources of trench parallel anisotropy in the Cascadia subduction system. The presence of B-type fabric in the mantle wedge or trench parallel flow beneath the slab would add a strong trench parallel component to a broader range of frequencies, making it difficult to constrain the source depths of the inferred chlorite-induced anisotropy. The generally trench perpendicular geometry of anisotropic fast directions in the wedge and subslab mantle beneath Cascadia means that other potential contributors to trench parallel anisotropy

are not present to obscure the contribution of these inferred hydrous phases. We further note that the high temperatures associated with the warm Cascadia slab likely act to reduce the otherwise stronger effect of similar antigorite-induced trench parallel anisotropy present in cooler subduction zones (e.g., Ryukyu) [Kneller *et al.*, 2008; Katayama *et al.*, 2009]. We suggest that in other subduction zones, while there may be a contribution to trench parallel anisotropy from other mechanisms, this is in addition to, not instead of, the effects of hydration within and just above the downgoing slab.

[18] Our results also have important implications for the interpretation of anisotropy in other tectonic settings where sheared hydrous phases may be present. For example, Mesozoic and earlier transpressional terrane boundaries in the eastern United States may preserve hydrous phases along ancient fault zones [Wagner *et al.*, 2012], and these phases may play an important role in controlling the local anisotropic signal in the vicinity of such faults. Recognizing the influence of hydrous phases on seismic anisotropy will improve our understanding of mantle flow patterns in subduction systems and may also provide a novel means to identify otherwise obscured terrane boundaries at depth.

[19] **Acknowledgments.** We thank D. Forsyth for access to his inversion codes. LSW was supported in part by NSF grant EAR-0809192. The High Lava Plains project was funded through NSF award EAR-0507248 (MJF) and EAR-0506914 (DEJ). MDL acknowledges support from an Alfred P. Sloan Research Fellowship. We thank Manuele Faccenda and Martha Savage for helpful reviews.

[20] The Editor thanks Manuele Faccenda and Martha Savage for their help in evaluating this paper.

References

- Audet, P. (2013), Seismic anisotropy of subducting oceanic uppermost mantle from fossil spreading, *Geophys. Res. Lett.*, *40*, 173–177, doi:10.1029/2012GL054328.
- Bezacier, L., B. Reynard, J. D. Bass, C. Sanchez-Valle, and B. V. Van de Moortele (2010), Elasticity of antigorite, seismic detection of serpentinites, and anisotropy in subduction zones, *Earth Planet. Sci. Lett.*, *289*, 198–208.
- Bostock, M. G., R. D. Hyndman, S. Rondenay, and S. M. Peacock (2002), An inverted continental Moho and serpentinization of the forearc mantle, *Nature*, *417*, 536–538.
- Currie, C. A., J. F. Cassidy, and R. D. Hyndman (2001), A regional study of shear wave splitting above the Cascadia subduction zone: Margin-parallel crustal stress, *Geophys. Res. Lett.*, *28*, 659–662.
- Currie, C. A., J. F. Cassidy, R. D. Hyndman, and M. G. Bostock (2004), Shear wave anisotropy beneath the Cascadia subduction zone and western North American craton, *Geophys. J. Int.*, *157*, 341–353.
- Faccenda, M., L. Burlini, T. V. Gerya, and D. Mainprice (2008), Fault-induced seismic anisotropy by hydration in subducting oceanic plates, *Nature*, *455*, 1097–1101.
- Forsyth, D. W., and A. Li (2005), Array analysis of two-dimensional variations in surface-wave phase velocity and azimuthal anisotropy in the presence of multipathing interference, in *Seismic Earth: Array Analysis of Broadband Seismograms*: Geophys. Monogr. Ser., vol. 157, edited by A. Levander, and G. Nolet, pp. 81–98, AGU, Washington DC.
- Hacker, B. R. (2008), H₂O subduction beyond arcs, *Geochem., Geophys., Geosyst.*, *9*, Q03001, doi:10.1029/2007GC001707.
- Healy, D., S. M. Reddy, N. E. Timms, E. M. Gray, and A. V. Brovarone (2009), Trench-parallel fast axes of seismic anisotropy due to fluid-filled cracks in subducting slabs, *Earth Planet. Sci. Lett.*, *283*, 75–86.
- Jung, H. (2011), Seismic anisotropy produced by serpentine in mantle wedge, *Earth Planet. Sci. Lett.*, *307*, 535–543.
- Jung, H., and S. Karato (2001), Water-induced fabric transitions in olivine, *Science*, *293*, 1460–1463.
- Jung, H., W. Mo, and H. W. Green (2009), Upper mantle seismic anisotropy resulting from pressure-induced slip transition in olivine, *Nat. Geosci.*, *2*, 73–77.
- Karato, S., H. Jung, I. Katayama, and P. Skemer (2008), Geodynamic significance of seismic anisotropy of the upper mantle: new insights from laboratory studies, *Annu. Rev. Earth Planet. Sci.*, *36*, 59–95.
- Katayama, I., K.-I. Hirauchi, K. Michibayashi, and J.-I. Ando (2009), Trench-parallel anisotropy produced by serpentine deformation in the hydrated mantle wedge, *Nature*, *461*, 1114–1117.
- van Keken, P. E., B. R. Hacker, E. M. Syracuse, and G. A. Abers (2011), Subduction factory: 4. Depth-dependent flux of H₂O from subducting slabs worldwide, *J. Geophys. Res.*, *116*, B01401, doi:10.1029/2010JB007922.
- Kneller, E. A., P. E. van Keken, S. Karato, and J. Park (2005), B-type olivine fabric in the mantle wedge: insights from high-resolution non-Newtonian subduction zone models, *Earth Planet. Sci. Lett.*, *237*, 781–797.
- Kneller, E. A., M. D. Long, and P. E. van Keken (2008), Olivine fabric transitions and shear wave anisotropy in the Ryukyu subduction system, *Earth Planet. Sci. Lett.*, *268*, 268–282.
- Long, M. D., and P. G. Silver (2008), The subduction zone flow field from seismic anisotropy: a global view, *Science*, *319*, 315–318.
- Mainprice, D., and B. Ildefonse (2009), Seismic anisotropy of subduction zone minerals – contribution of hydrous phases, in *Subduction Zone Geodynamics, Frontiers in Earth Sciences*, edited by S. Lallemand, and F. Funicello, pp. 63–84, Springer-Verlag, Berlin Heidelberg.
- Nedimovic, M. R., D. R. Bohnenstiehl, S. M. Carbotte, J. P. Canales, and R. P. Dziak (2009), Faulting and hydration of the Juan de Fuca plate system, *Earth Planet. Sci. Lett.*, *284*, 94–102.
- Nikulin, A., V. Levin, and J. Park (2009), Receiver function study of the Cascadia megathrust: Evidence for localized serpentinization, *Geochem. Geophys. Geosyst.*, *10*, Q07004, doi:10.1029/2009GC002376.
- Park, J., H. Yuan, and V. Levin (2004), Subduction zone anisotropy beneath Corvallis, Oregon: A serpentinite skid mark of trench-parallel terrane migration?, *J. Geophys. Res.*, *109*, B10306, doi:10.1029/2003JB002718.
- Peacock, S. M., K. Wang, and A. M. McMahon (2002), Thermal structure and metamorphism of subducting oceanic crust: Insight into Cascadia intraslab earthquakes, in *The Cascadia subduction zone and related subduction systems—Seismic structure, intraslab earthquakes and processes, and earthquake hazards: U.S. Geological Survey Open-File Report 02–328*, Geological Survey of Canada Open File 4350, edited by S. Kirby, et al., p. 17–24.
- Reynard, B. (2012), Serpentine in active subduction zones, *Lithos*, doi:10.1016/j.lithos.2012.10.012.
- Rondenay, S., M. G. Bostock, and J. Shragge (2001), Multiparameter two-dimensional inversion of scattered teleseismic body waves 3. Application to the Cascadia 1993 data set, *J. Geophys. Res.*, *106*, 30795–30807.
- Saito, M. (1988) DISPER80: a subroutine package for the calculation of seismic normal mode solutions, in *Seismic Algorithms: Computational Methods and Computer Programs*, edited by D. J. Doornbos, pp. 293–391, Elsevier, New York.
- Smith, R. B., and F. A. Dahlen (1973), The azimuthal dependence of Love and Rayleigh wave propagation in a slightly anisotropic medium, *J. Geophys. Res.*, *78*, 3321–3333.
- Song, T.-R. A., and Y. Kim (2012), Anisotropic uppermost mantle in young subducted slab underplating Central Mexico, *Nat. Geosci.*, *5*, 55–59.
- Wada, I., M. D. Behn, and A. M. Shaw (2012), Effects of heterogeneous hydration in the incoming plate, slab rehydration, and mantle wedge hydration on slab-derived H₂O flux in subduction zones, *Earth Planet. Sci. Lett.*, *353–354*, 60–71.
- Wagner, L., D. W. Forsyth, M. J. Fouch, and D. E. James (2010), Detailed three-dimensional shear wave velocity structure of the northwestern United States from Rayleigh wave tomography, *Earth Planet. Sci. Lett.*, *299*, 273–284.
- Wagner, L. S., M. D. Long, M. D. Johnston, and M. H. Benoit (2012), Lithospheric and asthenospheric contributions to shear-wave splitting observations in the southeastern United States, *Earth Planet. Sci. Lett.*, *341–344*, 128–138.
- Weeraratne, D. S., Forsyth, D. W., Yang, Y., and S. C. Webb (2007), Rayleigh wave tomography beneath intraplate volcanic ridges in the South Pacific, *J. Geophys. Res.*, *112*, B06303, doi:10.1029/2006JB004403.
- Yang, Y., and D. W. Forsyth (2006), Regional tomographic inversion of the amplitude and phase of Rayleigh waves with 2-D sensitivity kernels, *Geophys. J. Int.*, *166*, 1148–1160.